How grain size controls friction and wear in nanocrystalline metals

Ao Li and Izabela Szlufarska

Phys. Rev. B **92**, 075418 — Published 14 August 2015

DOI: 10.1103/PhysRevB.92.075418

How grain size controls friction and wear in nanocrystalline metals?

Ao Li[1] and Izabela Szlufarska[2]
[1]*Materials Science and Engineering,* [2]*Department of Materials Science & Engineering, University of Wisconsin.*

Abstract
Using molecular simulations we investigated the dependence of friction and wear on grain size in nanocrystalline copper. We found that effects of grain size are coupled to the effects of contact size, resulting in a transition from grain-size sensitive regime to grain size-insensitive regime in friction. This transition occurs because for small tips, friction-induced easy shear planes can be entirely accommodated in a single grain, rendering grain boundaries less relevant to sliding resistance. Trends in friction do not follow trends in hardness, which is sensitive to grain diameter in the entire grain size regime considered in this study. We have also discovered that coupling of the effects of grain diameter and contact size leads to an optimum grain size that minimizes formation of wear chips on the surface.

1. Introduction

Grain refinement to the nanometer regime has been shown to have important non-monotonic effects on mechanical properties of metals. Specifically, a number of studies reported existence of an optimum grain size that maximizes strength and hardness of metallic systems. [1, 2] This maximum strength corresponds to the grain diameter for which mechanisms of deformation transition from being dominated by intragranular dislocation plasticity to grain boundary (GB) sliding. In addition to this intrinsic grain size effect, mechanical properties can depend on the dimensions of the specimen – a so-called extrinsic size effect. For instance, mechanical strength of metallic nanopillars can be significantly lower [3] or higher [4] than the strength of the corresponding bulk samples.

Grain refinement has been also shown to be a highly promising path for improving friction and wear resistance of metals.[5, 6] However, despite these promising reports, at present the effects of grain size on wear and friction of nc metals are far from understood. For instance, it is unknown whether there is specific grain size that minimizes friction and wear or how the underlying mechanisms depend on the details of the microstructure. Molecular dynamics (MD) simulations have greatly contributed to discoveries of size effects in plasticity and of deformation mechanisms in nc metals during uniform shear, compression and during nanoindentation,[1, 2, 7-10] but MD simulations of wear of nc materials have only been reported in the last few years [11-13]. For example, the authors of Ref. [13] performed MD simulations of tip sliding on nc copper and discovered formation of folds in the worn material. This finding was supported by observations from atomic force microscopy (AFM) experiments. However, the grain size effect on friction and wear and on the underlying mechanisms of deformation were not explored in that study.

2. Simulation Methods

To address the question of size effects in friction and wear of face-centered cubic (fcc) metals, we perform a series of large-scale MD simulations of frictional sliding between a rigid parabolic tip and nc Cu (Fig. 1a) with grain diameter d ranging from 5 to 50 nm. Our simulation setup mimics AFM experiments of single-asperity friction. MD simulations were conducted with the LAMMPS software [14] using the embedded atoms method force field [15]. Voronoi algorithm was used to generate samples with grain diameter between 5 nm and 50 nm, corresponding to 26-76 million atoms in each sample. Grain sizes distribution is close to the Gaussian distribution (Fig. 1b), which is consistent with typical grain size distribution in nc copper.[16] Dimensions of samples with different grain diameters are listed in Table 1. Before any mechanical testing each nc sample is relaxed at 300K for 1ns.

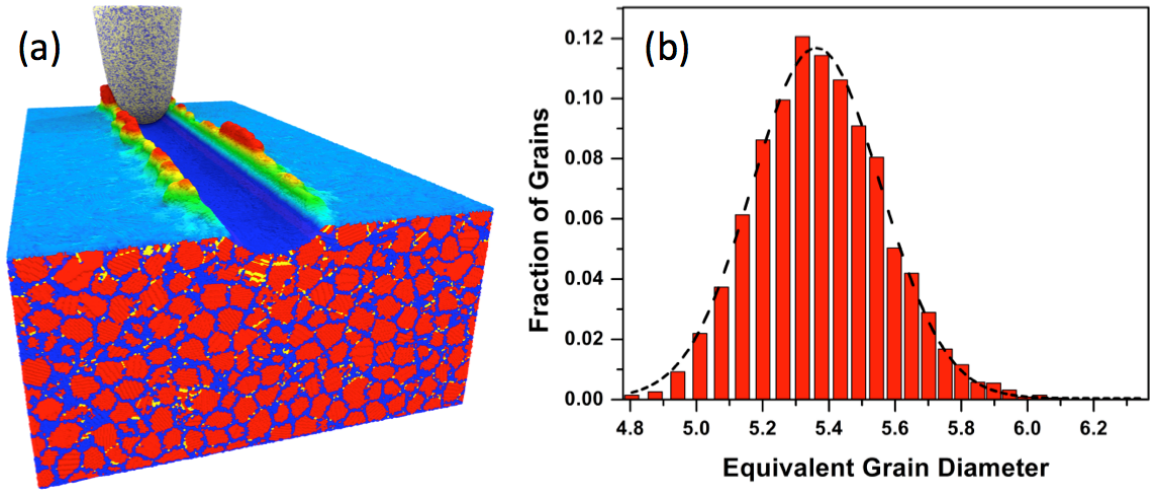

FIG. 1 (Color online). (a) Tip sliding over nc-Cu with d=5nm. (b) Grain size distribution of the sample with d=5nm. Equivalent grain diameter is determined by calculating total number of atoms in a given grain and then calculating the diameter assuming the grain is spherical. Black dashed line shows the Gaussian fitting with R^2= 0.995.

Table 1 *Sample dimensions and sizes for nc-Cu with different average grain diameters d.*

Grain Diameter *d* (nm)	Length (nm)	Width (nm)	Height (nm)	Number of Atoms
5.0	168	42	42	2,4409,623
15.0	170	42	42	2,537,0194
20.8	170	42	42	25,506,752
30.0	170	43	43	25,611,232
40.0	170	57	57	45,640,021
50.0	177	71	71	74,407,958

In order to test the mechanical properties of the samples, uniaxial tension and compression tests are performed at 300K for true strains up to 0.14 and with a deformation rate of $5 \times 10^8 s^{-1}$. Flow stress is defined as the average stresses in the true strain interval between 0.11 and 0.14, where the stress fluctuates around an approximately constant value. Dependence of flow stresses on grain diameter is shown in Fig. 2a and it exhibits a maximum between 10 nm and 15 nm. We confirmed that the presence of maximum is the result of transition from regime dominated by dislocation plasticity (large grain size) to regime dominated by GB sliding (small grain size), as shown in Figs. 2b-c.

It has been reported in literature that the transition from Hall-Petch relation to inverse Hall-Petch relation can be affected by thermal annealing of samples and relaxation of grain boundaries in MD simulations.[17] To verify that our results are not affected by thermal annealing and that our grain boundaries are relaxed, we have further annealed the nc-Cu samples at 1000K for 1 ns. The samples were then cooled down to room temperature and relaxed for another 1ns. Uniaxial tests on the samples annealed at

300K and at 1000K are shown in Fig. 2a. No significant difference was found in mechanical properties between the two types of samples, except for the sample with 5 nm grain diameter. The reason underlying the change in strength of the 5 nm sample is the grain growth, which is indicated by the significant decrease in fraction of GBs to atoms in crystalline grains (Fig. 2d).

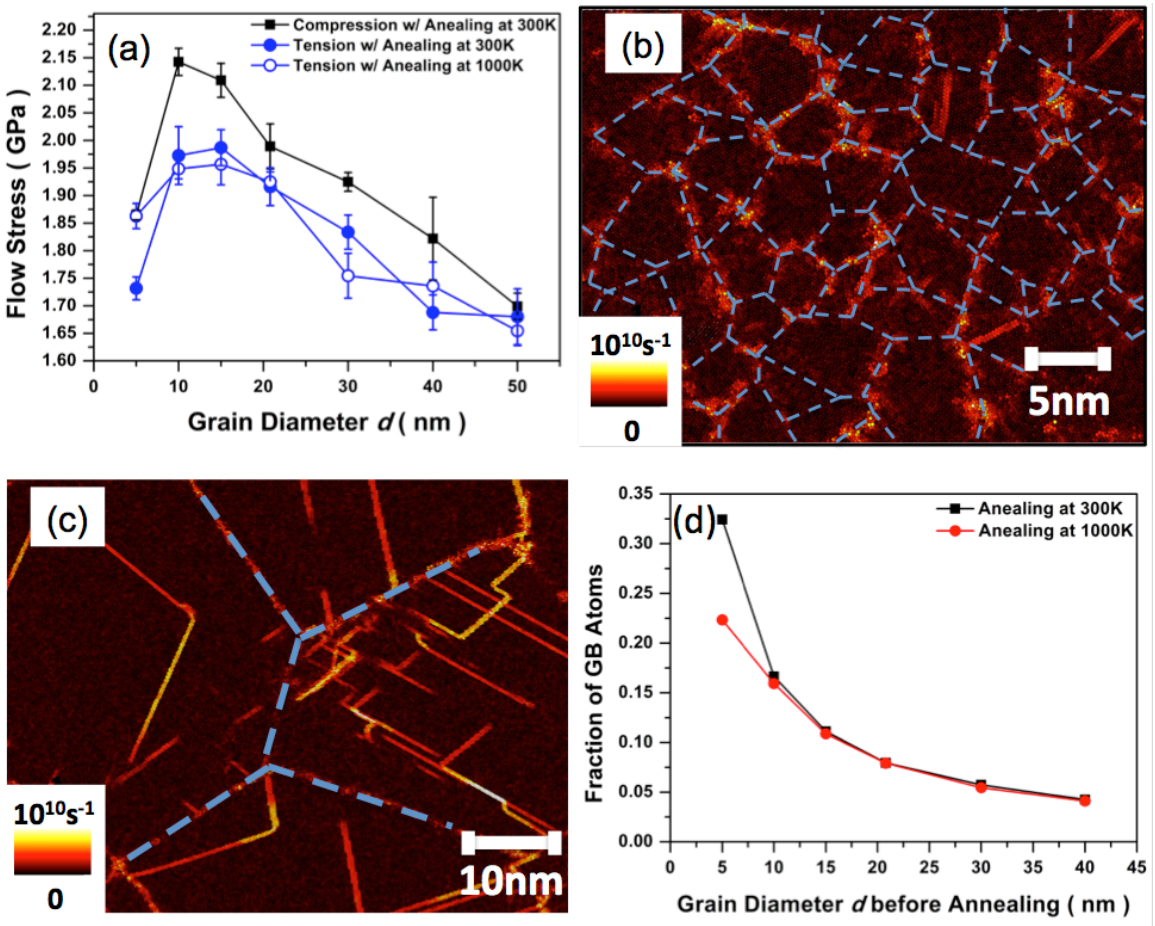

FIG. 2 (Color online) Uniaxial deformation and annealing effects. (a) Dependence of flow stress on grain diameter d. Error bars correspond to a standard deviation from a mean value calculated in the regime where flow stress reaches a plateau as a function of strain. (b) and (c) Local shear strain rate in samples with grain size 5 nm and 40 nm, respectively. Blue dashed lines are added to indicate the positions of GBs. (d) Fraction of GB atoms in the entire sample as a function of the nominal grain size for two annealing temperatures. GB atoms were identified using common neighbor analysis [18].

During sliding simulations, atoms in the bottom 1nm region and the 1nm thick vertical region far away from the sliding tip are kept fixed (frozen) to provide rigid boundaries. The temperature is controlled using a velocity-rescaling algorithm in a 3nm-thick thermostat layer of atoms adjacent to the bottom frozen layer. Sliding simulations are performed at 300K.

The tip is prepared from a melt-quenched amorphous SiC by cutting out a spherical shell, which is 3 nm thick, has the radius of cap curvature of 10 nm and the

height of 40 nm. The shell is relaxed at 300K for 200ps. In preparation of the amorphous SiC, we used the environment-dependent interatomic potential [19]. Tip-substrate interactions are described by Lennard-Jones potential [20], using the parameters: $\sigma_{Cu-Si} = 0.3039\text{nm}, \varepsilon_{Cu-Si} = 0.029\text{eV}$, $\sigma_{Cu-C} = 0.2869\text{nm}, \varepsilon_{Cu-Si} = 0.031\text{eV}$. These parameters were determined using Lorentz–Berthelot rules, $\sigma_{ij} = \frac{\sigma_i + \sigma_j}{2}$ and $\varepsilon_{ij} = \sqrt{\varepsilon_i \times \varepsilon_j}$ based on published parameters for pure Si, C [21], and Cu [22].

During sliding simulations, the tip is held rigid and it is moved laterally across the sample's surface with a velocity of 50 m/s. Simulations are performed at cutting depths between 1 nm and 11 nm. Maximum temperature observed at the contact interface is 390.1K and therefore it is not expected to have any significant impact on the results. The friction force and the normal forces are calculated by summing up all the forces acting on the tip in the lateral and normal directions, respectively. All reported properties correspond to averages calculated over at least 130 nm of sliding (after an initial equilibration period). These properties are first plotted as a function of normal load (see Figs. S3a-d in Supplemental Material [23]). To obtain the value of a given property at all loads, we linearly interpolate data between the measured points. By taking cross-sections at different loads (see vertical lines in Figs. S3a-d in Supplemental Material [23]) we can make plots of measured properties as a function of grain size. Crystallographic arrangement of atoms (fcc, hcp, or other) was determined using the common neighbor analysis [18].

3. Results and Discussion

A. Friction Coefficient

We have first calculated hardness *H* by dividing the average normal force *L* by the projected contact area *S*, both calculated during simulations of sliding. *H* was found to have a maximum at *d* = 30 nm (Fig. 3a), where *d* is the grain size averaged over the entire sample. One should note that the grain size near the surface is smaller than in the bulk because of the way the samples were prepared. The presence of the maximum in *H* is in qualitative agreement with trends in uniaxial deformation of nc Cu previously reported in literature [1] and reproduced in our simulations (Fig. 2a). We have also calculated friction coefficient μ, which is defined as the friction force divided by the normal load. The results are plotted in Fig. 3b as a function of grain diameter. We find that μ initially decreases with increasing *d*, but then becomes insensitive to it. μ is inversely proportional to *H* for grains smaller than ~30 nm (Fig. 3c). Because $\mu = F/L$ and $H = L/S$, we can calculate the lateral hardness $\tau = F/S = \mu H$, which is a constant if μ is inversely proportional to *H.* Thus provided that τ is constant, at the same normal load, *S* is smaller for harder materials, leading to a decreased resistance to sliding (μ) with increasing *H*. This is consistent with the traditional understanding of friction-hardness relation. However, it is interesting to note that for larger grains, we found that μ and *H* are no longer inversely proportional to each other, which suggests that in this regime deformation mechanisms responsible for vertical hardness may be different than deformation mechanisms controlling friction.

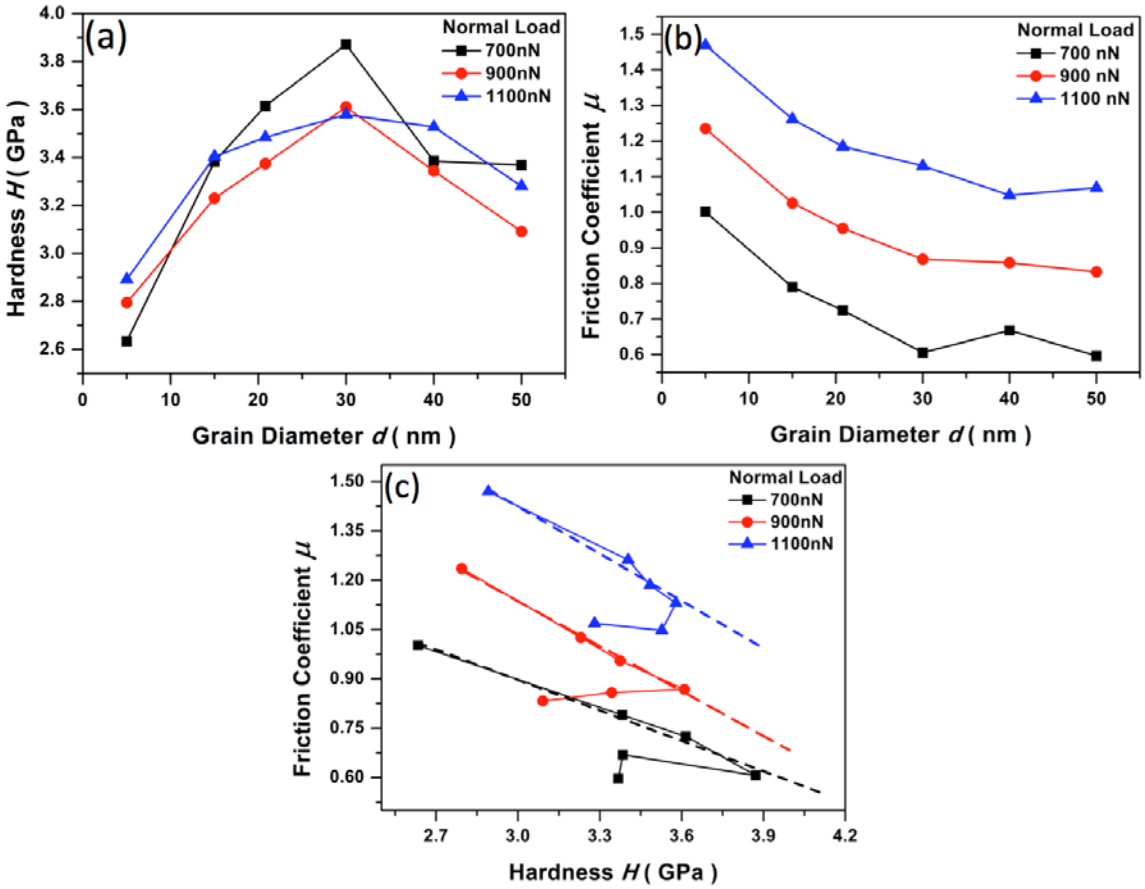

FIG. 3 (Color online). (a) Hardness and (b) Friction coefficient as a function of grain size. (c) Friction coefficient vs. Hardness. Dashed lines correspond to expected linear trends.

While deformation mechanisms that govern the decrease of hardness with increasing d in the larger grain size regime are already reasonably well understood in the context of the Hall-Petch relation [24, 25], mechanisms that govern friction and its dependence on d are still unknown. To analyze the latter mechanisms, in Fig. 4a we show a cross-sectional view of the contact and we color code atoms based on their velocity component parallel to the sliding direction. Displayed velocities are averages calculated over 100 ps of sliding. The region outlined by points *ABEDC* represents the deformation regime of the Cu sample, which separates the undeformed material (below the *CDE* line) and the chip (above the *AB* line). There is essentially no plastic flow in the chip, except for a small amount of shear along the chip-tip contact line, which shear is generally ignored in this type of analysis.[26] In other words, almost all deformation takes place inside the *ABEDC* region and it is the shear in this region that accommodates frictional sliding and controls the friction force. Within this region one can identify slip lines (the *CD* line is one of them), which are lines of constant velocity and which are parallel to the axes of maximum shear stress.[26]

So far we have not discussed how the geometric slip lines are related to the underlying structure of the nc Cu. To find such relations, in Figs. 4b and 4c we show distributions of local strain rate in samples with d = 5 nm and 30 nm, respectively.

Details of strain rate calculations can be found in Ref. [23]. For the 5 nm sample, the grain size is much smaller than the tip size. The tip-induced deformation regime encompasses multiple grains and plasticity proceeds by coordinated shearing in different directions along multiple GBs. Dislocation glide in the grain interior is inhibited by the dense network of GBs and there are no extended dislocation slips observed in our system. In contrast, in the 30 nm sample, where grain diameter is larger than tip size, deformation occurs partially or entirely in one grain and it is localized along a well-defined slip line. We will refer to this extended and relatively straight slip line as an easy-shear plane because it is expected to provide a lower resistance to shear than the meandering path of short-range shear events that accommodate tip-induced deformation in the 5 nm sample. One can now understand why friction transitions from grain size sensitive regime to grain size insensitive regime as the d increases. For $d \leq 30$ nm, both hardness and friction of nc Cu in our simulations are controlled by GB sliding as well as some limited dislocation activity inside the grains (Fig. 2b), which results in hardness and the friction coefficient being linearly dependent on one another (Fig. 3c). For larger grains, hardness is controlled by intragranular dislocations and their propensity to pile-up at the GBs (Fig. 2c), which mechanism is grain size dependent. Friction on the other hand is accommodated by formation of an easy-shear plane inside a single grain, which mechanism is not directly related to hardness and to a large extent is independent of the grain size.

We found two types of mechanisms to be responsible for formation of an easy-shear plane inside a crystalline grain. The first mechanism operates when one of the planes from the {111} family is parallel or almost parallel to the direction of the geometric slip line (Fig. 4d). Partial dislocations propagate on the {111} plane, leaving behind a stacking fault (or a twin boundary), which in turn provides a plane with low resistance to shear. The second mechanism involves formation of a new GB along the geometric slip line (Fig. 4e), which is the result of a pile-up of dislocations (either statistically stored or geometrically necessary). Continued sliding is accommodated by development of parallel easy shear-planes as shown in Fig. 4f.

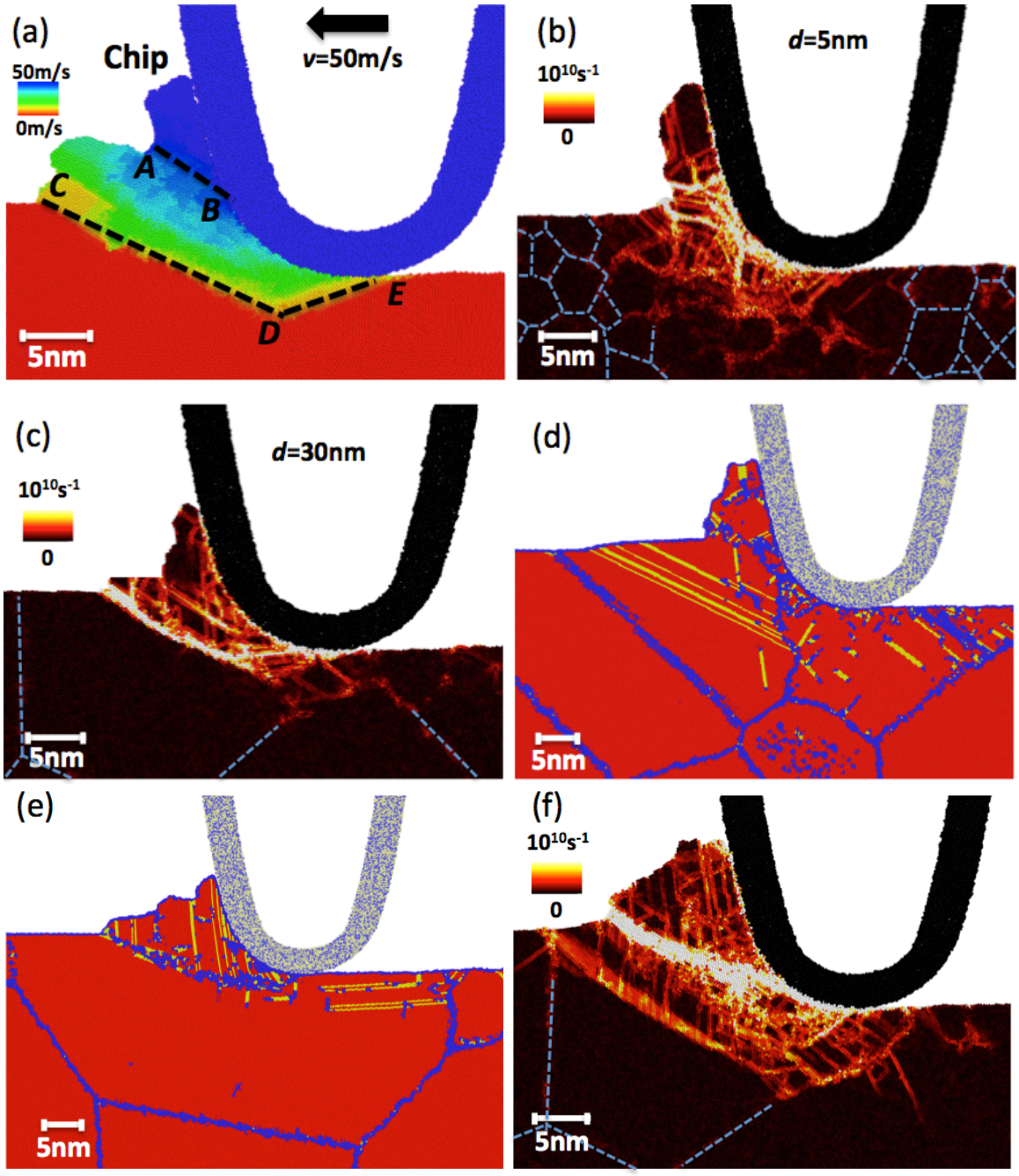

FIG. 4 Cross-sectional views of the contact area: (a) Atoms are color-coded by their lateral velocities. Dashed lines are slip-lines representing lines of constant lateral velocity. (b) and (c) Local shear strain rate in samples with grain size d=5 and 30 nm, respectively. Formation of (d) stacking faults and twin boundaries (yellow) and (e) a new GB (blue) in fcc Cu (red). (f) Formation of two parallel easy-shear planes. Colors represent the same local shear strain rate as in (b) and (c). Grain size in (d) and (f) is d=40 nm and in (e) d=50nm. Blue dashed lines in (b), (c), and (f) are added to indicate the positions of GBs away from the deformation region.

As discussed above, for the case where the tip size is small as compared to the grain size, there is a clearly defined slip line that develops inside individual grains during frictional sliding. This slip line is accommodated either by formation of twin boundaries and stacking faults (Fig.4d) or by formation of a new GB (Fig.4e). Here, we show that there are two general mechanisms of such GB formation. One involves pile-up of dislocations in the region of the slip line, which is a line parallel to the direction of the highest shear stress based on the geometry of the sample. The dislocations are nucleated at the surface of the sample or are emitted from existing GBs. The entangled dislocations in the pile-up rearrange to form a new GB and provide a plane of easy slip. This mechanism is illustrated in Fig. 5a and Video S1a. The second mechanism involves formation of geometrically necessary dislocations due to bending of the grain by the sliding tip. This mechanism is shown in Fig. 5b and Video S1b, where an array of geometrically necessary partial dislocations evolves into a new GB.

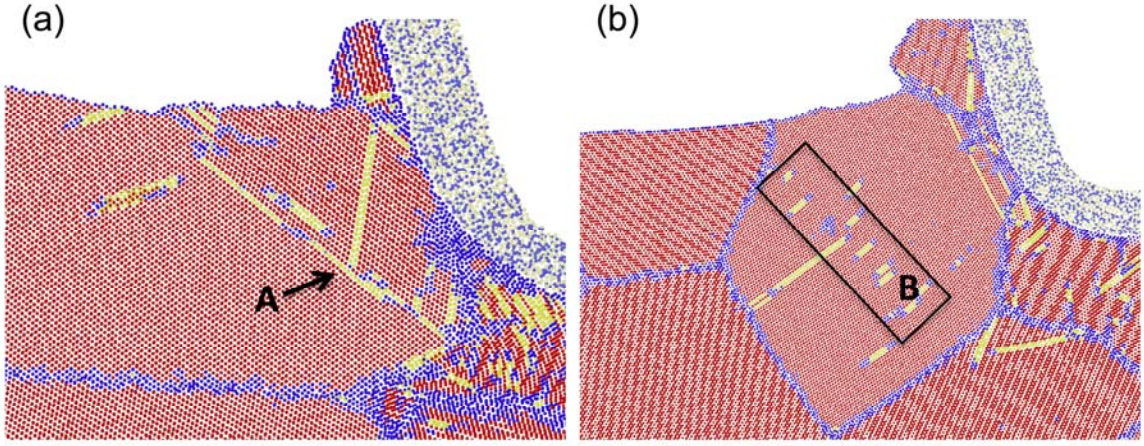

FIG. 5 Mechanisms of friction-induced GB formation. (a) Glide of partial dislocations nucleated at the surface is hindered (at location A) by a twin boundary parallel to the direction of the geometric slip line. (b) Formation of an array of geometrically necessary partial dislocations in region B. In both (a) and (b), fcc Cu atoms are shown in red. Yellow Cu atoms have hcp structure and represent stacking faults and twin boundaries. Blue represents those Cu atoms that do not have either fcc or hcp structure. Tip atoms are colored in white and light blue.

B. Wear

How does wear of nc Cu depend on the grain size? In general wear can refer either to surface damage or to loss of material during sliding.[27] During tip sliding, surface material may be effectively displaced to the two sides of the groove and it may not accumulate in front of the tip. This wear mode is called plowing and it only leads to ridges and grooves left in the wake of the tip. Although in this case material is displaced, no chip formation or material loss takes place during sliding. In other words, wear does happen but there is no material loss. The displaced volume V_{disp} is a useful measure to quantify this type of wear.

In another case, displaced material can accumulate in front of the tip and form a chip. This wear mode is referred to as cutting. Chips only attach loosely to the surface and can easily become wear debris by fracturing with the help of small external force.

Fracture often occurs at weak connections between the chip and the surface. It is much easier for chips in the cutting mode to become wear debris than for groove ridges to turn into debris in the plowing mode. As a result, chips can be regarded as precursors of wear debris. [26, 28]

In experiments, tip vibration, irregular tip shape, and other external force during sliding will initiate the fracture and turn chips into surface debris. In our simulations, we do not apply such external forces, since this is not the focus of our study. As a result chip removal does not take place in simulations, but chips are still precursors of wear debris and the chip volume V_{chip} is a reasonable measure to quantify such form of wear.

One important property of the chip material is that it is pushed forward by a tip and it moves together with a tip. Based on this property, one can use the velocity of each atom onto the sliding direction as the criterion for determining which atoms belong to the chip (blue atoms in Fig. 4a and Fig. 6a). It is interesting to note that the pile-up and chips have nc structure and form GBs, which is illustrated in Fig. 6b.

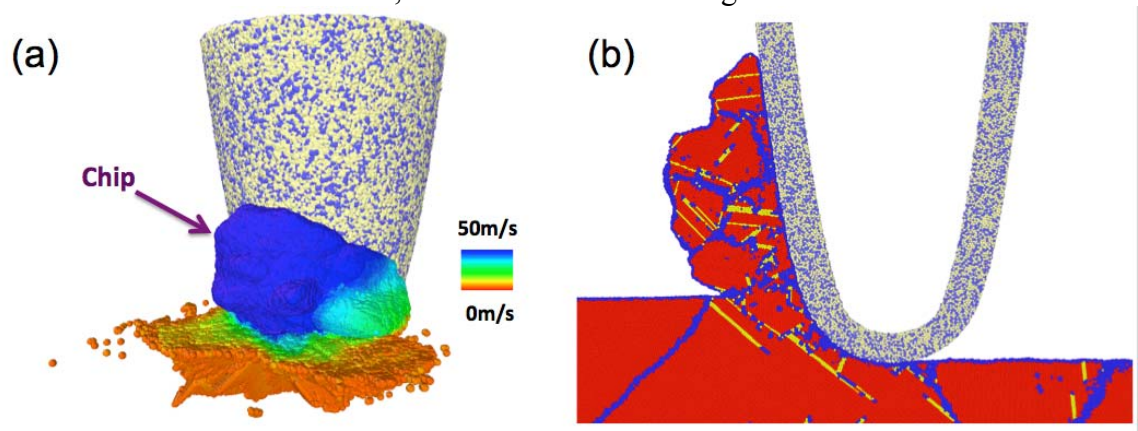

FIG. 6 (a) Chip formation in our simulations. Sample atoms are color-coded by their lateral velocities. (b) Formation of GBs inside the pile-up. Grain diameter is 40 nm and the average normal load is 1120nN. Color scheme is the same as in Fig. 5.

We first quantify surface damage by calculating the total volume of displaced material V_{disp}^{tot} above the original surface of the sample after 130nm of sliding distance. V_{disp}^{tot} includes the pile-up in front of the tip and the plowed material behind it (Fig. 1a). This analysis is essentially equivalent to the measurements of groove volume or groove depth that are widely used in ball-on-disk wear tests [6] and nanoscratch experiments [29]. As shown in Fig. 3a, V_{disp}^{tot} first decreases with increasing d (in the small grain size regime) and then it becomes approximately constant (in the larger grain size regime). It is perhaps not surprising that the dependence of V_{disp}^{tot} on d during sliding (Fig. 7a) qualitatively resembles the trend in μ (Fig. 3b), because larger friction leads to more displaced volume [23]. In the large d regime, frictional sliding is accommodated by slip along an easy-shear plane inside a crystalline grain, where the size and position of the easy-shear plane depend on the contact geometry and are to a large extent independent of d. Slip along the easy-shear plane controls both the resistance to sliding (i.e., the friction coefficient) and the displaced volume.

What is unexpected, however, is the trend with d that we found for the average chip volume V_{chip} (Fig. 7b). Because chips are regarded as precursors of wear debris, V_{chip}

is one of the accepted ways to quantify wear-induced material loss. In our simulations, chip atoms are identified as having almost the same lateral velocity as the tip (atoms above the AB line in Fig. 4a and blue atoms in Fig. 7a). Chip volumes reported in Fig. 7b are averaged over the sliding distance.

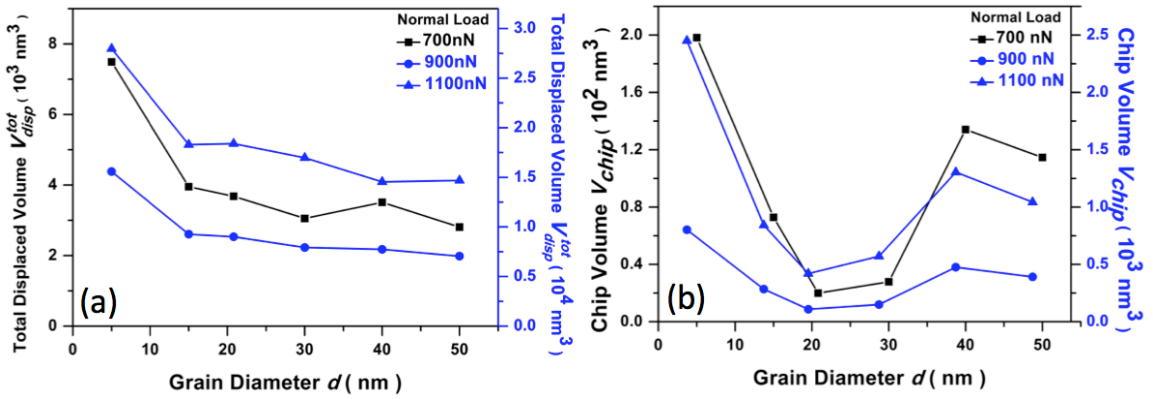

FIG. 7 (Color online). Dependence of wear on grain diameter d. (a) Volume of total displaced material after 130nm of sliding distance. (b) Average chip volume during tip sliding.

We find (Fig. 7b) that there is an optimum grain size (~20 nm) that minimizes V_{chip}. There are two factors that contribute to V_{chip}, which are mass flux into the chip and mass flux out of the chip. Mass flux into the chip is controlled by hardness and since it is more difficult to displace a hard material, mass flux into the chip is smaller for harder materials. Interestingly, the mass flux out of the chip is controlled not only by hardness, but also by another mechanism that can reduce the chip volume. This mechanism is cracking of the pile-up (Fig. 8a and 8b), which increases the flow of displaced material to the back of the tip. Cracking in turn is influenced by the anisotropy of the pile-up material because the more anisotropic the pile-up, the easier it is to initiate a crack. Grain size plays an important role in cracking because it is responsible for the anisotropy of the pile-up (see Fig. 8a,b and Supplemental Material [23]) and because cracking occurs primarily along GBs (Fig. 6b).

To quantify pile-up anisotropy, we define an anisotropy factor A as the product of the two terms $A = \left|\frac{\sum_0^n \theta \times N_\theta}{\sum_0^n N_\theta}\right| \times \sqrt{\frac{\sum(\frac{N_\theta - N_0}{N_0})^2}{n}}$. N_θ stands for the number of atoms in a vertical slice of the pile-up, which slice forms a polar angle θ with the direction of sliding. N_0 is the value of N_θ averaged over all n slices. Anisotropy factor A captures both, the deviation of the pile-up's center of mass from the sliding direction and fluctuation of the number of atoms among the different slices [23]. As shown in Fig. 8c, A has a maximum at d~20 nm, which explains why chip volume is minimized for this grain size.

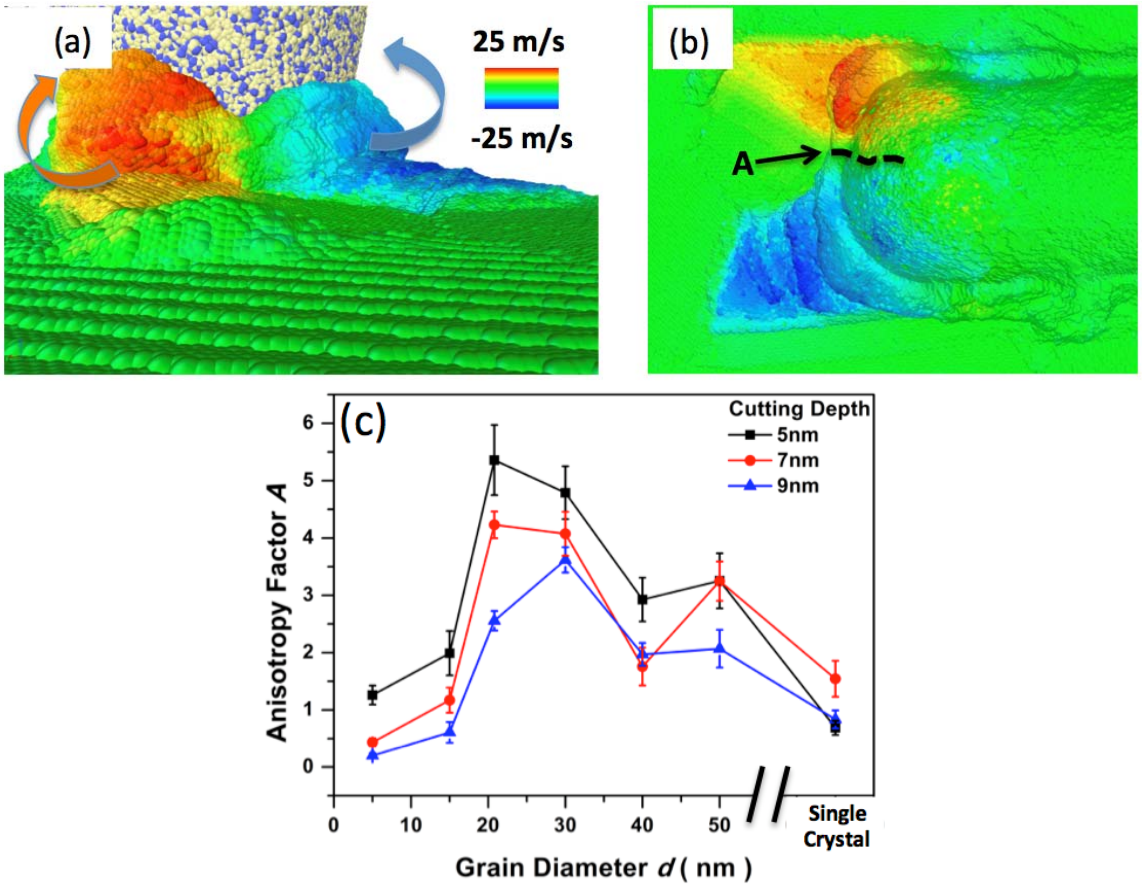

FIG.8 (Color online) Anisotropy of pile-up: (a) Perspective view and (b) top view. Atoms are color-coded by their velocity component perpendicular to the sliding direction. In (b), the region marked as A shows where cracking initiates and the dashed line denotes crack propagation path. (c) Anisotropy factor A as a function of grain size d for three different cutting depths. Cutting depth is defined as the vertical distance between the lowest point on the tip and the undamaged surface of the sample. The reported values of A are averages calculated over at least 130 nm of the sliding distance and error bars are defined as a standard deviation from the mean.

The reason why A has a maximum at d~20 nm is a coupling between the grain size and the size of the cutting tool. Specifically, the diameter of the projected area of the tip is ~20 nm. For larger grain sizes (single crystal being an extreme case), the wavelength of heterogeneity that results from the grain structure of the material is too large to have a significant influence on the anisotropy on the length scale probed by the tip. In this case the tip is most of the time plowing through a single crystal grain with sporadic encounters of GBs. For smaller grain sizes (amorphous material being an extreme case), the wavelength of the grain heterogeneity is small compared to the tip size and even if small cracks develop, they do not propagate and do not fracture the pile-up as effectively as observed in the case of intermediate grain sizes.

In order to further test the hypothesis that A is maximized when the tip size and the grain diameter are comparable, we fix the grain size and change the diameter of the tip. For this purpose, we use a series of cylindrical tips with diameters d_{tip} that range from

4 nm to 28 nm and we perform scratch simulations on nc-Cu samples with average grain diameter of 15 nm and a cutting depth of 7 nm (Fig. 9a). To avoid stress concentrations at tip corners, we blunt the corners of the tip so that the radius of curvature of the corner *r* is 2 nm. Cylindrical tips are used instead of parabolic tips with a spherical cap in order to eliminate the effect of tip-attack-angle, which varies with the diameter of a parabolic tip and which is expected to have a significant effect on pile-up and chip formation during cutting.

We also introduce the ratio $k = \frac{S_g}{S_t}$. Here, S_g is the average cross-sectional area of grains intersected by the surface plane. It is measured as the ratio between the total surface area and the total number of grains observed on the surface. S_t is the cross-sectional area of the tip within the plane of the surface. Grain and tip sizes are comparable when *k* is close to 1. Dependence of *A* on *k* for 7nm cutting depth is shown in Fig. 9b. One can see that *A* is maximized when $k \approx 1$ for both cases considered in this study: changing the grain diameter and keeping the size of the tip constant and changing the diameter of the tip and keeping the grain size constant.

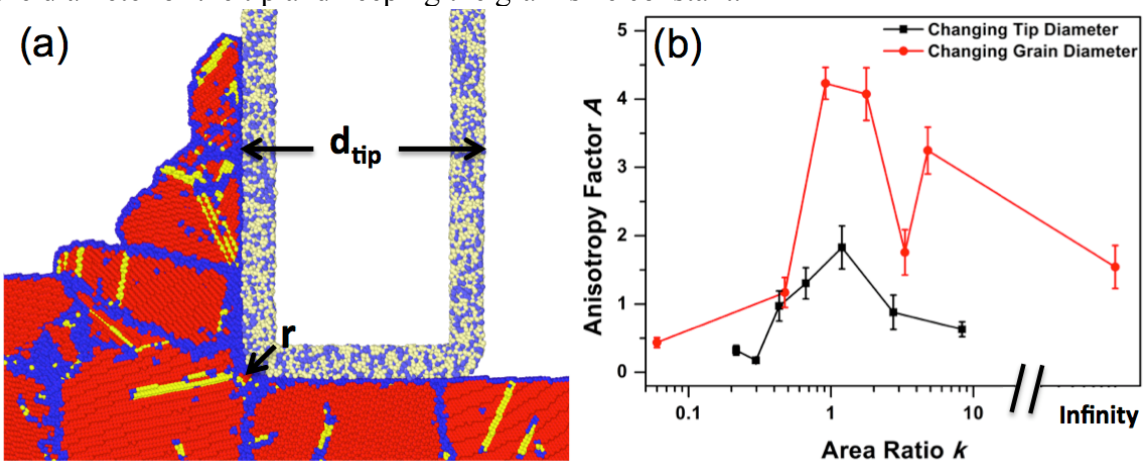

FIG. 9 (Color online) (a) A cylindrical tip made of amorphous SiC with a diameter d_{tip} cutting a copper sample with grain diameter 15nm at a cutting depth of 7nm. Colors have the same meaning as in Fig. 6. (b) Dependence of anisotropy factor A on the area ratio k. The reported values of A are averages calculated over at least 130 nm of the sliding distance and error bars are defined as a standard deviation from the mean.

4. Conclusions

Our results demonstrate that size-effects in friction and wear depend on both, intrinsic (grain size) and extrinsic (contact size) factors. When the average grain size is smaller than tip sizes, friction coefficient is inversely proportional to hardness. When the grain size is larger than the tip, friction coefficient becomes insensitive to hardness. The lack of dependence of μ on hardness is due to a newly found mesoscopic deformation mechanism, which is formation of an easy-shear plane. Surface damage first decreases with increasing hardness (in the small grain size regime) and then becomes insensitive to hardness (in the large grain size regime). We also found that there is a grain diameter that minimizes material loss. This effect is also due to a coupling of grain size and tip size,

which coupling can maximize pile-up anisotropy and therefore maximize the volume of the chip.

References:

1. J. Schiotz, and K. W. Jacobsen, *Science* **301**, 1357-1359 (2003).
2. J. Schiotz, F. D. Di Tolla, and K. W. Jacobsen, *Nature* **391**, 561-563 (1998).
3. D. Jang, and J. R. Greer, *Scripta Materialia* **64**, 77-80 (2011).
4. J. Y. Kim, D. Jang, and J. R. Greer, *Scripta Materialia* **61**, 300-303 (2009).
5. Z. N. Farhat, Y. Ding, D. O. Northwood, and A. T. Alpas, *Mat Sci Eng a-Struct* **206**, 302-313 (1996).
6. Y. S. Zhang, Z. Han, K. Wang, and K. Lu, *Wear* **260**, 942-948 (2006).
7. E. M. Bringa, A. Caro, Y. Wang, M. Victoria, J. M. McNaney, B. A. Remington, R. F. Smith, B. R. Torralva, and H. Van Swygenhoven, *Science* **309**, 1838-1841 (2005).
8. H. Van Swygenhoven, *Science* **296**, 66-67 (2002).
9. K. W. Jacobsen, and J. Schiotz, *Nat Mater* **1**, 15-16 (2002).
10. V. Yamakov, D. Wolf, S. R. Phillpot, A. K. Mukherjee, and H. Gleiter, *Nat Mater* **1**, 45-49 (2002).
11. M. Mishra, and I. Szlufarska, *J Mater Sci* **48**, 1593-1603 (2013).
12. M. Mishra, C. Tangpatjaroen, and I. Szlufarska, *Journal of the American Ceramic Society* **97**, 1194-1201 (2014).
13. N. Beckmann, P. A. Romero, D. Linsler, M. Dienwiebel, U. Stolz, M. Moseler, and P. Gumbsch, *Physical Review Applied* **2**, 064004 (2014).
14. S. Plimpton, J Comput Phys **117**, 1-19 (1995).
15. Y. Mishin, M. J. Mehl, D. A. Papaconstantopoulos, A. F. Voter, and J. D. Kress, *Physical Review B* **63**, 224106 (2001).
16. K. M. Youssef, R. O. Scattergood, K. L. Murty, and C. C. Koch, *Applied Physics Letters* **85**, 929-931 (2004).
17. N. Q. Vo, R. S. Averback, P. Bellon, A. Caro, *Physical Review B* **78**, 241402 (2008).
18. D. Faken, H. Jónsson, *Computational Materials Science* **2**, 279-286 (1994).
19. J. F. Justo, M. Z. Bazant, E. Kaxiras, V. V. Bulatov, and S. Yip, *Physical Review B* **58**, 2539-2550 (1998).
20. J. E. Jones, *Proceedings of the Royal Society of London. Series A* **106**, 463-477 (1924).
21. N. Rajabbeigi, B. Elyassi, T. T. Tsotsis, and M. Sahimi, *J Membrane Sci* **335**, 5-12 (2009).
22. P. Guan, D. R. Mckenzie, and B. A. Pailthorpe, *J Phys-Condens Mat* **8**, 8753-8762 (1996).
23. See Supplemental Material at [] for additional description of methods, data, concepts, and analysis of the large-scale simulations.
24. E. O. Hall, *Proceedings of the Physical Society. Section B* **64**, 742 (1951).
25. N. J. Petch, *The Cleavage Strength of Polycrystals*. (J. Iron Steel Inst., London, 1953), vol. 173.
26. M. C. Shaw, *Metal Cutting Principles*. (Clarendon Press, Oxford, 1984).

27. B. Bhushan, *Principles and Appliations of Tribology*. (A John Wiley & Sons Ltd., New York, ed. 2, 2013).
28. D. A. Stephenson, and J. S. Agapiou *Metal Cutting Theory and Practice*. (Marcel Dekker,Inc., New York, 1997).
29. Y.-R. Jeng, P.-C. Tsai, and S.-H. Chiang, *Wear* **303**, 262-268 (2013).